Letter

Hydrogen anion as a strong magnetic mediator for obtaining high-temperature ferromagnetic semiconductors: The case of hydride double perovskites

Chao Jia,[1,2] Xingxing Li,[1,2,3,4,*] Qunxiang Li,[1,2,3,4,†] and Jinlong Yang[1,2,3,4]

[1]*Key Laboratory of Precision and Intelligent Chemistry, University of Science and Technology of China, Hefei, Anhui 230026, China*
[2]*Department of Chemical Physics, University of Science and Technology of China, Hefei, Anhui 230026, China*
[3]*Hefei National Research Center for Physical Sciences at the Microscale, University of Science and Technology of China, Hefei, Anhui 230026, China*
[4]*Hefei National Laboratory, University of Science and Technology of China, Hefei, Anhui 230026, China*

(Received 8 July 2022; revised 10 October 2022; accepted 20 March 2023; published 6 April 2023)

Realizing ferromagnetic (FM) semiconductors with Curie temperatures (T_c) above 300 K is highly desirable for spintronics but remains a big challenge. Up to now, the oxide double perovskite La_2NiMnO_6 is regarded as one of the most promising FM semiconductors, where the near-180° strong superexchange interaction brings its T_c up to 280 K, but it is still below room temperature. Here, we propose that, by using H^- instead of O^{2-} as magnetic mediator, the resulted perfect 180° bond angle and short interaction distance between magnetic ions can notably raise the T_c beyond 300 K. The idea is verified by theoretically designing a class of thermodynamically stable hydride double perovskites A_2NiVH_6 (A = Na, K, Rb, Cs) with ferromagnetic T_c up to 789 K. Moreover, the A_2NiVH_6 are identified as intriguing bipolar magnetic semiconductors with the carrier's spin orientation readily reversible by electrical gating. In addition, the possible Ni/V disorder further changes A_2NiVH_6 to be compensated ferrimagnetic semiconductors with vanishing magnetization, which may have unique advantages in antiferromagnetic spintronics.

DOI: 10.1103/PhysRevB.107.L140404

Ferromagnetic (FM) semiconductors are the cornerstones of spintronic devices due to their broad prospects in magnetic field sensors [1], magnetic random access memories [2], spin field-effect transistors [3], etc. Ferromagnetic semiconductors include intrinsic ferromagnetic semiconductors such as EuX (X = O, S, Se, Te) [4,5], ACr_2X_4 (A = Cd, Hg; X = S, Se) [6], $BiMnO_3$ [7], La_2NiMnO_6 [8], $CrGeTe_3$ [9], CrI_3 [10], and diluted magnetic semiconductors such as (Ga,Mn)As [11]. Unfortunately, most known FM semiconductors have Curie temperatures significantly lower than room temperature, making them difficult to put into practical applications. Note that in the community of diluted magnetic semiconductors, several groups have previously claimed to obtain ferromagnetism at room temperature, but these observations remain heavily debated [12–15].

Double perovskites $A_2BB'X_6$ (X = O, Cl, Br, I) with variable element combinations serve as fertile soils for exploring intrinsic FM semiconductors [8,16–19]. Among them, La_2NiMnO_6 with near-room-temperature ferromagnetism ($T_c \sim 280$ K), large magnetroresistance, and colossal magnetodielectricity is an outstanding representative. Due to its excellent electronic and magnetic properties, La_2NiMnO_6 possesses great potentials in spintronics, multiferroics, and electrocatalysis [20–26]. The high T_c of La_2NiMnO_6 originates from the near-180° (160° on average) $d^8(Ni^{2+}) - p(O^{2-}) - d^3(Mn^{4+})$ FM superexchange interactions [8]. Considering that the Curie temperature of La_2NiMnO_6 is still below room temperature, developing ferromagnetic double perovskites with $T_c > 300$ K and good semiconducting properties is urgently required for practical applications.

On the other hand, owing to the rich physical and chemical properties, metal hydrides play important roles in various fields such as hydrogen storage, energy conversion, organic synthesis, catalysis, and high-temperature superconductivity [27–29]. For example, the metal hydride LaH_{10} has been confirmed in experiment as a superconductor with a rather high critical temperature of 250 K [29]. However, almost all metal hydrides studied so far are nonmagnetic and their potential in designing functional spintronic materials remains largely unexplored.

In this Letter, we demonstrate that robust ferromagnetic semiconductors with Curie temperatures well above 300 K can be achieved in double perovskites simply by exploiting H instead of O as intervening magnetic mediators. The idea is confirmed by theoretically designing a series of thermodynamically stable hydride double perovskites A_2NiVH_6 (A = Na, K, Rb, Cs) with extremely high Curie temperatures (up to 789 K).

According to the Goodenough-Kanamori rules [30–32], the 180° superexchange interaction between $t_{2g}^6 e_g^2 (d^8)$ and $t_{2g}^3 e_g^0 (d^3)$ is ferromagnetic (Fig. 1). In real materials, the angle between magnetic ions may deviate from 180° due to phonon instability, causing a notable decrease of the superexchange strength, such as in La_2NiMnO_6. To enhance the superexchange interaction, one needs to (1) make the angle

*lixx@ustc.edu.cn
†liqun@ustc.edu.cn

 ©2023 American Physical Society

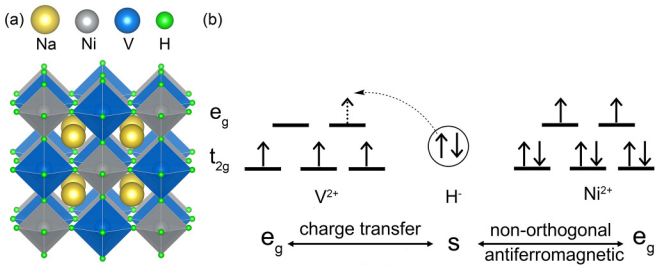

FIG. 1. (a) Structure of Na_2NiVH_6. (b) Schematic diagram of Ni-H-V superexchange interaction.

between magnetic ions reach 180° as much as possible and (2) shorten the interaction distance between magnetic ions. Taking the structure of La_2NiMnO_6 (space group 14) as the starting point, we find that when O^{2-} is replaced by H^-, one or both of the above conditions can be satisfied. Note that, in order to maintain the charge balance of the system, La^{3+} in La_2NiMnO_6 should be replaced by alkali metal elements $Li^+/Na^+/K^+/Rb^+/Cs^+$. Meanwhile, to keep the d^8-d^3 electronic configurations, $Mn^{4+}(d^3)$ is replaced by $V^{2+}(d^3)$. Therefore, the chemical formula of the obtained hydride double perovskites is A_2NiVH_6 (A = Li, Na, K, Rb, and Cs).

To evaluate whether these compounds can form stable perovskite structures, the Goldschmidt tolerance factors (t) [33] expressed as

$$t = \frac{r_A + r_H}{\sqrt{2}\left[\left(\frac{r_{Ni}+r_V}{2}\right) + r_H\right]} \quad (1)$$

are calculated. The Shannon ionic radii are used for all ions except H^-, which is assumed to have a radius of 140 pm [34]. Empirically, compounds with tolerance factors between 0.81 and 1.11 can crystallize in perovskite structures, and those with tolerance factors close to 1 are likely to have a perfect cubic structure. We find that when A = Li, Na, K, Rb, Cs, the tolerance factors of A_2NiVH_6 are 0.77, 0.92, 1.00, 1.02, and 1.08, respectively. Therefore, A_2NiVH_6 have the potential to form cubic perovskites, except for Li_2NiVH_6, which possesses a too small tolerance factor and is discarded in the following studies. Using the distorted La_2NiMnO_6 (space group 14) structure as the initial structure, after fully structural optimization, all A_2NiVH_6 relax to cubic structures with the $FM\bar{3}M$ space group (group 225), which is consistent with the prediction by tolerance factors. Furthermore, test calculations on other commonly seen perovskite phases confirm that the cubic phase is the most energetically favorable in the double perovskite family [see the Supplemental Material [35] for details (see, also, Refs. [36–48] therein)]. Thus the superexchange angle between magnetic ions changes from 160° in La_2NiMnO_6 to perfect 180° in A_2NiVH_6. The structure of cubic Na_2NiVH_6 is shown in Fig. 1(a). The lattice constants of unit cell Na_2NiVH_6, K_2NiVH_6, Rb_2NiVH_6, and Cs_2NiVH_6 are 7.231, 7.669, 7.913, and 8.225 Å (Table I), respectively. Compared with Ni-Mn distance (3.871 Å on average) in La_2NiMnO_6, the Ni-V spacing becomes shorter when the A site is Na (3.614 Å) or K (3.835 Å), while it is somewhat larger for A = Rb (3.957 Å), Cs (4.113 Å).

To confirm that H behaves as an anion and is similar to O within the perovskites, we calculate the electron occupation numbers by integrating the projected density of states and perform Bader charge analysis for O in La_2NiMnO_6 and H in Na_2NiVH_6 (Fig. S1 in the Supplemental Material [35]). The spin-up and spin-down electron occupation numbers of *p* orbitals of O are 2.79 and 2.80, respectively. And Bader charge analysis shows each O accepts 1.20 negative charges, which is consistent with the −2 valence state of O. As a comparison, the spin-up and spin-down occupation numbers for H are 0.73 and 0.68, respectively. And Bader charge analysis shows each H accepts 0.53 negative charges, indicating that the valence state of H is −1.

TABLE I. Lattice constant (a), enthalpy of formation (ΔH_f) at 10 GPa, band gap (E_g), effective mass (m^*), and Curie temperature (T_c). m_e is the mass of an electron.

	a (Å)	ΔH_f (meV/atom)	E_g (eV)	m^* (m_e)	T_c (K)
Na_2NiVH_6	7.231	−246	0.89	CBM:Γ → X:0.92	789
				M → K:1.49	
				VBM:K → V:0.98	
				V → Γ:0.78	
K_2NiVH_6	7.669	−320	1.15	CBM:Γ → X:0.99	568
				M → K:2.72	
				VBM:K → V:1.16	
				V → Γ:1.28	
Rb_2NiVH_6	7.913	−263	1.18	CBM:Γ → X:0.86	489
				M → K:2.14	
				VBM:K → V:1.29	
				V → Γ:1.08	
Cs_2NiVH_6	8.225	−130	1.12	CBM:Γ → X:0.73	410
				M → K:2.17	
				VBM:K → V:0.95	
				V → Γ:0.89	

To evaluate whether the proposed hydride double perovskites are experimentally synthesizable, we calculate their formation enthalpies (ΔH_f) under different pressures, which are defined by

$$\Delta H_f = H_{A_2NiVH_6} - \left(2H_A + H_{Ni} + H_V + 3H_{H_2}\right), \quad (2)$$

where H_X (X = A_2NiVH_6, A, Ni, V, H_2) represent the enthalpies of the corresponding species. For A, Ni, V, and H_2, the enthalpy of the most stable element crystal is used. As shown in Fig. 2(a), without pressure, all compounds have positive ΔH_f except Na_2NiVH_6 (−31 meV/atom). When the pressure increases to 10 GPa, the ΔH_f of all compounds become negative, i.e., −246, −320, −263, and −130 meV/atom for Na_2NiVH_6, K_2NiVH_6, Rb_2NiVH_6, and Cs_2NiVH_6, respectively. This indicates the hydride double perovskite could be fabricated at about 10 GPa. Note that such a pressure is achievable during experimental synthesis [49–51]. Up to now, some hydride perovskites have been synthesized, such as $NaMgH_3$, which is prepared via standard solid-state method, by reacting NaH and MgH_2 powders (1:1 ratio) at 623 K under 7 MPa H_2 pressure [52]. It is possible that A_2NiVH_6 could be prepared in a similar way, i.e., by heating the mixture of AH, NiH_2, and VH_2 powders at certain temperature and H_2 pressure.

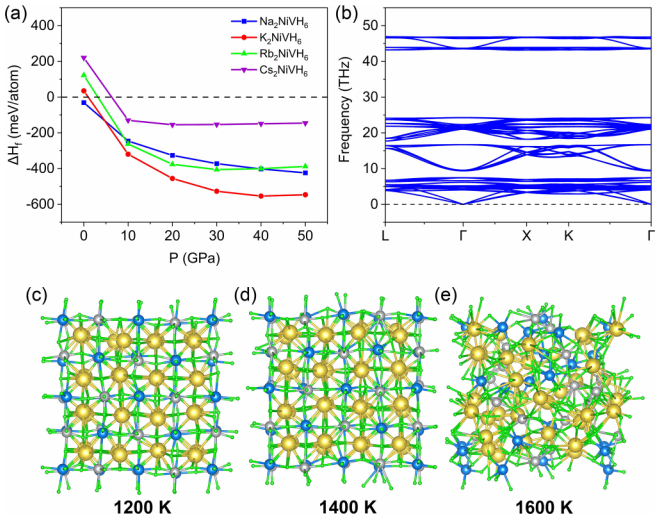

FIG. 2. (a) Calculated formation enthalpies (ΔH_f) as a function of pressure for Na_2NiVH_6, K_2NiVH_6, Rb_2NiVH_6, and Cs_2NiVH_6. (b) The phonon spectrum of Na_2NiVH_6. (c)–(e) The structural snapshots of Na_2NiVH_6 after 10 ps *ab initio* molecular dynamics (AIMD) simulation under the temperature of 1200, 1400, and 1600 K, respectively.

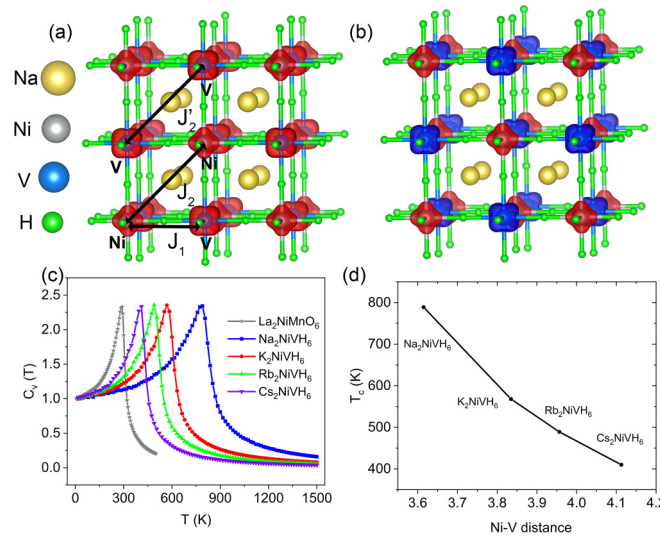

FIG. 3. Spin density distribution of Na_2NiVH_6 in (a) ferromagnetic and (b) ferrimagnetic states. Spin up and spin down are indicated by red and blue, respectively. (c) The simulated specific heat C_v with respect to temperature for La_2NiMnO_6 and A_2NiVH_6 (A = Na, K, Rb, Cs). (d) The predicted T_c of A_2NiVH_6 as a function of Ni-V distance.

To examine whether there are other competing phases, a global structural search for Na_2NiVH_6 is performed based on particle swarm optimization implemented in the CALYPSO code [53–55]. Results show the cubic double perovskite is only a metastable phase with its enthalpy 96 meV/atom higher than that of the most stable phase (see the Supplemental Material [35] for details). Nevertheless, it is theoretically proposed that metastable phases with energies within 200 meV/atom compared to the most stable phase are possible to synthesize, with the help of substrates, defects, and temperature [56]. Experimentally, many metastable perovskites have been synthesized [57–59].

To explore the dynamic stability of A_2NiVH_6, phonon spectrum calculations are performed [Fig. 2(b) and Figs. S4-S5]. No obvious imaginary frequency is found in all structures, indicating that these structures are local minima on the potential energy surface and dynamically stable. *Ab initio* molecular dynamics simulations at standard pressure are further employed to examine the thermal stability of Na_2NiVH_6 at 1200, 1400, and 1600 K. The structure snapshots in Figs. 2(c)–2(e) demonstrate that Na_2NiVH_6 has a high thermal stability and the structure can be retained at the temperature up to 1400 K. These results imply that once the cubic double perovskites are synthesized, they can exist stably at normal temperature and pressure without decomposing into other phases.

To confirm the ferromagnetic superexchange between $Ni^{2+}(d^8)$ and $V^{2+}(d^3)$ in A_2NiVH_6, four magnetic orders, i.e., ferromagnetic (FM), antiferromagnetic (AFM), ferrimagnetic-I (FIM-I), and ferrimagnetic-II (FIM-II) (Fig. S7), are computed. The results indicate that all A_2NiVH_6 indeed possess the ferromagnetic ground state, consistent with the Goodenough-Kanamori rules. The spin density distribution of Na_2NiVH_6 in FM and FIM-I states are shown in Figs. 3(a) and 3(b), from which one can see that the magnetic moments in Na_2NiVH_6 are mainly contributed by Ni^{2+} and V^{2+} ions. The Curie temperatures are further estimated by employing the Monte Carlo simulations based on the classical Heisenberg Hamiltonian [60]

$$H = -\sum_{i,j} J_{ij} S_i S_j, \tag{3}$$

$$J_1 = -\frac{E_{\mathrm{FM}} - E_{\mathrm{FIM}-I}}{48 S_i S_j}, \tag{4}$$

$$J_2 = -\frac{E_{\mathrm{FIM}-I} - E_{\mathrm{FIM}-II} - 24 J_1 S_i S_j}{32 S_i S_i}, \tag{5}$$

$$J_2' = -\frac{E_{\mathrm{FIM}-II} - E_{\mathrm{AFM}} + 8 J_1 S_i S_j}{32 S_j S_j}, \tag{6}$$

where J_1 is the nearest $Ni^{2+} - V^{2+}$ exchange parameter and $J_2(J_2')$ is the nearest $Ni^{2+} - Ni^{2+}$ ($V^{2+} - V^{2+}$) exchange parameter; $S_i = 1$ and $S_j = 3/2$ are the spins of Ni^{2+} and V^{2+}, respectively. From the energies of different magnetic states calculated by PBE+U ($U_{\mathrm{eff}} = 3$ eV), we deduce that $J_1 = 31.56$ meV and $J_2(J_2') = -1.05(-0.38)$ meV for Na_2NiVH_6. Since $J_2(J_2')$ is at least an order of magnitude smaller than J_1, it is omitted in the following Monte Carlo simulations. To obtain T_c, the specific heat $C_v = (\langle E^2 \rangle - \langle E \rangle^2)/T^2$ is calculated after the system reaches its equilibrium at a given temperature. Then the T_c is determined as the temperature where the $C_v(T)$ peak occurs. The simulated $C_v(T)$ curves are shown in Fig. 3(c) and the obtained T_c are summarized in Table I. The T_c of all A_2NiVH_6 are much higher than room temperature, with Na_2NiVH_6 possessing the highest $T_c \sim 789$ K. As a comparison, based on the same parameter extraction method, the Curie temperature of La_2NiMnO_6 is predicted to be 289 K, consistent with the experiment

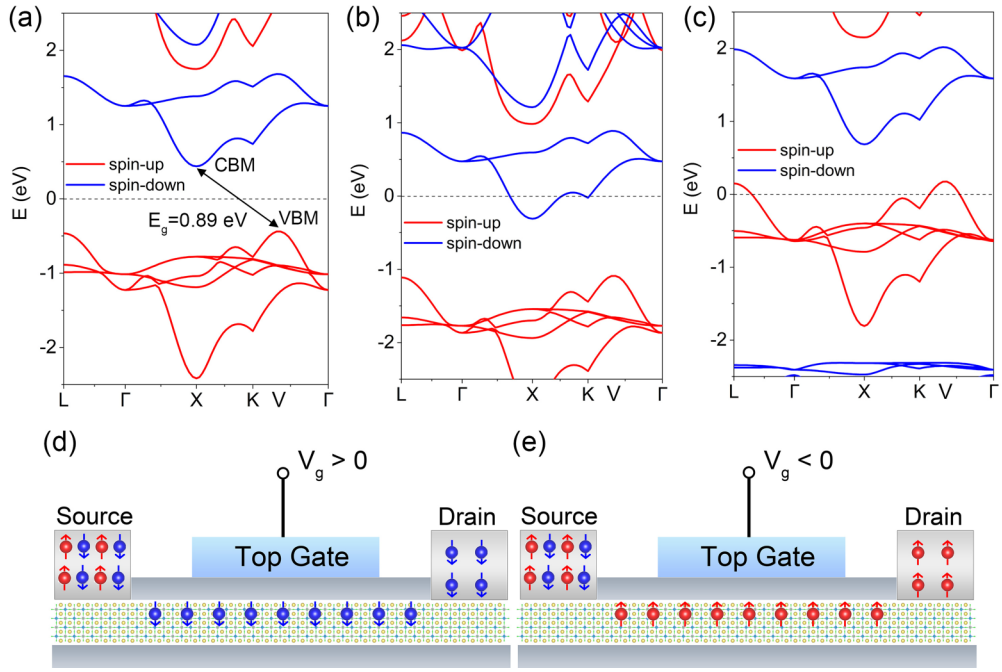

FIG. 4. Band structures of Na_2NiVH_6 (a) without doping and doping with (b) 0.25 electrons or (c) 0.25 holes per primitive cell. Schematic of spin channel switching when (d) positive or (e) negative gate voltage is applied. Fermi levels are set to zero.

(280 K). In addition, we also calculate the Curie temperatures of Na_2NiVH_6 under different U values (U_{eff} = 2–5 eV; T_c = 663–852 K) and HSE06 functional (T_c = 805 K), ensuring that the high Curie temperature is an intrinsic property of the system and not sensitive to the calculation methods (see the Supplemental Material [35] for details). Figure 3(c) shows the variation of the T_c of A_2NiVH_6 with the Ni-V distance, from which one can see that, as the Ni-V distance increases, the T_c of the compounds decreases. For Na_2NiVH_6 and K_2NiVH_6, the high-T_c ferromagnetism originates from both the perfect 180° superexchange angle and short Ni-V distance, while for Rb_2NiVH_6 and Cs_2NiVH_6, although the Ni-V distance is somewhat longer than La_2NiMnO_6, the perfect 180° superexchange angle still makes their T_c significantly higher than 300 K.

The total and element resolved electronic band structures of A_2NiVH_6 are calculated by PBE+U (U_{eff} = 3 eV) method to investigate their electronic properties [Fig. 4(a) and Figs. S11-S14]. All A_2NiVH_6 are ferromagnetic semiconductors with an indirect band gap of 0.89, 1.15, 1.18, and 1.12 eV for Na_2NiVH_6, K_2NiVH_6, Rb_2NiVH_6, and Cs_2NiVH_6, respectively. As a comparison, the band gap of La_2NiMnO_6 calculated by PBE+U (U_{eff} = 3 eV) method is 1.23 eV (the experimental gap is about 1.5 eV) [61]. The CBM of A_2NiVH_6 appears at the X point in the reciprocal space and the VBM emerges between the K and Γ points (labeled as V point). The element resolved band structures in Fig. S11 show that the VBM of Na_2NiVH_6 is mostly contributed by H and Ni, and CBM is mainly constructed by Ni, respectively. The minimum electron and hole effective masses at the CBM or VBM are all less than 1 m_e (Table I), indicating good semiconducting properties. As is known, the formation of small polarons may seriously lower the mobility of carriers. Therefore, to investigate whether small polarons are formed, we insert one electron into Na_2NiVH_6 and perform an *ab initio* molecular dynamics simulation with a 2 × 2 × 1 supercell for 2 ps. Every 200 fs we calculate the density of states and partial charge density at the CBM (Fig. S15). No apparent lattice distortion is found during simulation. The density of states of all structures show no drop in energy levels at the CBM and no localized trap states are formed in the gap. The partial charge densities also demonstrate that the inserted electron is not localized. These results suggest no small polaron formation in our system. Furthermore, we introduce symmetry breaking in the system by respectively shortening a Ni-H bond or a V-H bond at one atomic site and perform two AIMD runs for a longer period of 8 ps (Fig. S16). The results suggest the absence of polarons as well. It should be pointed out that, although PBE+U calculations show no formation of polarons in Na_2NiVH_6, the presence of polarons can still not be excluded when using more advanced functionals, such as hybrid functionals.

Importantly, all A_2NiVH_6 exhibit the feature of bipolar magnetic semiconductors with the VBM and CBM fully spin polarized in the opposite spin direction [62–68]. This unique electronic structure provides a feasible method to control the carriers' spin polarization direction simply by applying a gate voltage. When the Fermi level is shifted around the CBM after electron doping at a positive gate voltage, the carriers are 100% spin-down polarized [Fig. 4(b)], while they change to be 100% spin-up polarized under hole doping when a negative gate voltage moves the Fermi level towards the VBM [Fig. 4(c)]. By this way, the conduction spin channel of A_2NiVH_6 can be easily switched between spin up and spin

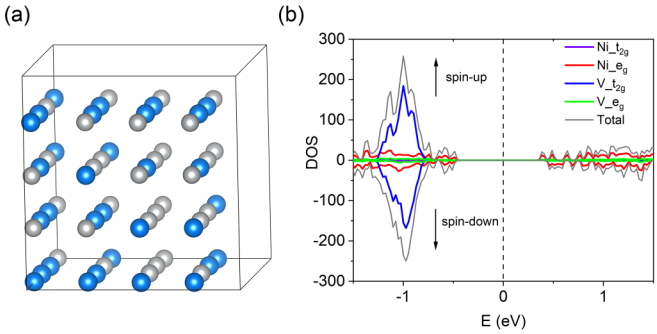

FIG. 5. (a) Generated special quasirandom structure (SQS) for Na_2NiVH_6 with Na and H atoms omitted. (b) Total and orbital projected density of states (DOS) for SQS. Fermi levels are set to zero.

down via reversing the gate polarity [Figs. 4(d) and 4(e)]. Note that under both electron doping and hole doping, A_2NiVH_6 maintain the FM ground state (Table S2).

To further confirm the ferromagnetic semiconductor property of A_2NiVH_6, the electronic structures are further calculated by the HSE06 functional (Figs. S11-S14), which are qualitatively consistent with the results obtained by PBE+U, except that the band gaps predicted by HSE06 (2.58, 2.74, 2.77, and 2.67 eV for Na_2NiVH_6, K_2NiVH_6, Rb_2NiVH_6, and Cs_2NiVH_6, respectively) are larger than those by PBE+U. In addition, the band structure of Cs_2NiVH_6 changes to be a normal magnetic semiconductor with the same spin channel for VBM and CBM rather than a bipolar magnetic semiconductor.

In La_2NiMnO_6, due to the similar ionic radii of Ni^{2+} and Mn^{4+} (0.69 Å and 0.53 Å), partial B site disorder exists in experiment, which may also occur in A_2NiVH_6. Thus it is necessary to figure out the magnetic and electronic properties of A_2NiVH_6 when Ni-V disorder is present. To do this, a 320-atom special quasirandom structure (SQS) under complete B-site disorder is generated for Na_2NiVH_6 [Fig. 5(a)]. SQS is a method that aims to design a single finite special supercell whose average atomic correlation functions of the cluster best match those of the random alloys [69]. To determine the magnetic ground state of SQS, we calculate three magnetic configurations, including FM (all the magnetic moments are assigned as spin up), FIM (the magnetic moments of all Ni are assigned as spin down and those of V are assigned as spin up), and AFM (specify the magnetic moments according to the GK rules: all $Ni^{2+} - Ni^{2+}$ and $V^{2+} - V^{2+}$ coupling pairs are set as AFM and all $Ni^{2+} - V^{2+}$ coupling pairs are set as FM). Results show that the AFM state is most energetically favorable (Table S3 in the Supplemental Material [35]).

Further calculations reveal AFM SQS has a lower enthalpy than FM ordered structure, but their relative stability is inverted when SQS is in a FM state (Table S4). This indicates the competition of disordered and ordered structures depends on the magnetic state. There are several possible ways to minimize disorder as follows. (1) Using special growth techniques, such as laser molecular beam epitaxy. A typical example is given by La_2CrFeO_6 [70]. (2) Employing a suitable substrate during growth, as exemplified by La_2CoMnO_6 [71]. (3) Applying an external magnetic field to tune the magnetic state during growth. In experiment, there have been some relevant cases [72,73].

Now we turn to examine the electronic properties of the SQS in AFM state. Interestingly, despite a zero total magnetic moment, the SQS possesses spin polarization in the spin-up channel at both valence and conduction band edges [Fig. 5(b)]. This unique nature of magnetism in the SQS is consistent with the behavior of a fully compensated ferrimagnet with vanishing magnetization [74]. The orbital projected density of states [Fig. 5(b)] reveal the VBM and CBM are mainly contributed by Ni e_g orbitals. In addition, we generate another eight SQSs for Na_2NiVH_6 and find that, although the arrangement of Ni and V in different SQSs are different, they all have very similar total energies and exhibit the same properties of fully compensated ferrimagnets (Table S5 and Fig. S17). Furthermore, they are all magnetic semiconductors, though the spin polarization at VBM and CBM may be different (Fig. S17). The density of states averaged over nine SQSs keeps the behavior of a magnetic semiconductor with significant spin polarization around the Fermi energy level (Fig. S18).

In conclusion, by exploiting hydrogen anion as magnetic mediator, a class of high-T_c ferromagnetic semiconductors in hydride double perovskites A_2NiVH_6 (A = Na, K, Rb, Cs) is theoretically designed. The high Curie temperature originates from the strong superexchange interaction induced by the perfect 180° Ni-H-V bond angle and short Ni-V coupling distance. In addition, all A_2NiVH_6 are identified as bipolar magnetic semiconductors with great promise in electric field controlled spintronic devices. In the case of complete B site disorder, A_2NiVH_6 show a fully compensated ferrimagnetlike behavior, which may have unique advantages in antiferromagnetic spintronics. This work shows the potential of hydrogen anion as a strong magnetic mediator for realizing intrinsic ferromagnetic semiconductors with high Curie temperatures.

This work was supported by the National Natural Science Foundation of China (Grants No. 22288201, No. 22273092, and No. 21873088), by the Strategic Priority Research Program of the Chinese Academy of Sciences(Grant No. XDB0450101), by the Youth Innovation Promotion Association CAS (Grant No. 2019441), by the Anhui Initiative in Quantum Information Technologies (Grant No. AHY090400), by the Innovation Program for Quantum Science and Technology (Grant No. 2021ZD0303306), and by USTC Tang Scholar.

[1] H. P. Baltes and R. S. Popovic, Integrated semiconductor magnetic field sensors, Proc. IEEE **74**, 1107 (1986).

[2] S. Wolf, D. Awschalom, R. Buhrman, J. Daughton, S. von Molnár, M. Roukes, A. Y. Chtchelkanova, and D. Treger,

Spintronics: A spin-based electronics vision for the future, Science **294**, 1488 (2001).
[3] A. Fert, Nobel lecture: Origin, development, and future of spintronics, Rev. Mod. Phys. **80**, 1517 (2008).
[4] B. Matthias, R. Bozorth, and J. Van Vleck, Ferromagnetic Interaction in EuO, Phys. Rev. Lett. **7**, 160 (1961).
[5] I. N. Goncharenko and I. Mirebeau, Ferromagnetic Interactions in EuS and EuSe Studied by Neutron Diffraction at Pressures up to 20.5 GPa, Phys. Rev. Lett. **80**, 1082 (1998).
[6] P. Baltzer, P. Wojtowicz, M. Robbins, and E. Lopatin, Exchange interactions in ferromagnetic chromium chalcogenide spinels, Phys. Rev. **151**, 367 (1966).
[7] T. Kimura, S. Kawamoto, I. Yamada, M. Azuma, M. Takano, and Y. Tokura, Magnetocapacitance effect in multiferroic $BiMnO_3$, Phys. Rev. B **67**, 180401(R) (2003).
[8] N. S. Rogado, J. Li, A. W. Sleight, and M. A. Subramanian, Magnetocapacitance and magnetoresistance near room temperature in a ferromagnetic semiconductor: La_2NiMnO_6, Adv. Mater. **17**, 2225 (2005).
[9] C. Gong, L. Li, Z. Li, H. Ji, A. Stern, Y. Xia, T. Cao, W. Bao, C. Wang, Y. Wang *et al.*, Discovery of intrinsic ferromagnetism in two-dimensional van der waals crystals, Nature (London) **546**, 265 (2017).
[10] B. Huang, G. Clark, E. Navarro-Moratalla, D. R. Klein, R. Cheng, K. L. Seyler, D. Zhong, E. Schmidgall, M. A. McGuire, D. H. Cobden *et al.*, Layer-dependent ferromagnetism in a van der waals crystal down to the monolayer limit, Nature (London) **546**, 270 (2017).
[11] H. Ohno, n. A. Shen, a. F. Matsukura, A. Oiwa, A. Endo, S. Katsumoto, and Y. Iye, (Ga, Mn)As: A new diluted magnetic semiconductor based on GaAs, Appl. Phys. Lett. **69**, 363 (1996).
[12] T. Dietl, H. Ohno, F. Matsukura, J. Cibert, and D. Ferrand, Zener model description of ferromagnetism in zinc-blende magnetic semiconductors, Science **287**, 1019 (2000).
[13] T. Jungwirth, J. Sinova, J. Mašek, J. Kučera, and A. H. MacDonald, Theory of ferromagnetic (III, Mn)V semiconductors, Rev. Mod. Phys. **78**, 809 (2006).
[14] K. Sato, L. Bergqvist, J. Kudrnovský, P. H. Dederichs, O. Eriksson, I. Turek, B. Sanyal, G. Bouzerar, H. Katayama-Yoshida, V. A. Dinh, T. Fukushima, H. Kizaki, and R. Zeller, First-principles theory of dilute magnetic semiconductors, Rev. Mod. Phys. **82**, 1633 (2010).
[15] T. Dietl and H. Ohno, Dilute ferromagnetic semiconductors: physics and spintronic structures, Rev. Mod. Phys. **86**, 187 (2014).
[16] Q. Tao, P. Xu, M. Li, and W. Lu, Machine learning for perovskite materials design and discovery, npj Comput. Mater. **7**, 23 (2021).
[17] C. Lu, M. Wu, L. Lin, and J. Liu, Single-phase multiferroics: new materials, phenomena, and physics, Natl. Sci. Rev. **6**, 653 (2019).
[18] S. Vasala and M. Karppinen, $A_2B'B''O_6$ perovskites: A review, Prog. Solid State Chem. **43**, 1 (2015).
[19] X. Li, X. Wu, Z. Li, and J. Yang, Proposal of a general scheme to obtain room-temperature spin polarization in asymmetric antiferromagnetic semiconductors, Phys. Rev. B **92**, 125202 (2015).
[20] D. Choudhury, P. Mandal, R. Mathieu, A. Hazarika, S. Rajan, A. Sundaresan, U. V. Waghmare, R. Knut, O. Karis, P. Nordblad, and D. D. Sarma, Near-Room-Temperature Colossal Magnetodielectricity and Multiglass Properties in Partially Disordered La_2NiMnO_6, Phys. Rev. Lett. **108**, 127201 (2012).
[21] H. Das, U. V. Waghmare, T. Saha-Dasgupta, and D. D. Sarma, Electronic Structure, Phonons, and Dielectric Anomaly in Ferromagnetic Insulating Double Pervoskite La_2NiMnO_6, Phys. Rev. Lett. **100**, 186402 (2008).
[22] Y. Shiomi and E. Saitoh, Paramagnetic Spin Pumping, Phys. Rev. Lett. **113**, 266602 (2014).
[23] H. J. Zhao, W. Ren, Y. Yang, J. Íñiguez, X. M. Chen, and L. Bellaiche, Near room-temperature multiferroic materials with tunable ferromagnetic and electrical properties, Nat. Commun. **5**, 4021 (2014).
[24] M. Qu, X. Ding, Z. Shen, M. Cui, F. E. Oropeza, G. Gorni, V. A. de la Pena O'Shea, W. Li, D.-C. Qi, and K. H. Zhang, Tailoring the electronic structures of the La_2NiMnO_6 double perovskite as efficient bifunctional oxygen electrocatalysis, Chem. Mater. **33**, 2062 (2021).
[25] Y. Tong, J. Wu, P. Chen, H. Liu, W. Chu, C. Wu, and Y. Xie, Vibronic superexchange in double perovskite electrocatalyst for efficient electrocatalytic oxygen evolution, J. Am. Chem. Soc. **140**, 11165 (2018).
[26] A. Hossain, A. Atique Ullah, P. Sarathi Guin, and S. Roy, An overview of La_2NiMnO_6 double perovskites: synthesis, structure, properties, and applications, J. Sol-Gel Sci. Technol. **93**, 479 (2020).
[27] E. S. Wiedner, M. B. Chambers, C. L. Pitman, R. M. Bullock, A. J. Miller, and A. M. Appel, Thermodynamic hydricity of transition metal hydrides, Chem. Rev. **116**, 8655 (2016).
[28] A. J. Jordan, G. Lalic, and J. P. Sadighi, Coinage metal hydrides: synthesis, characterization, and reactivity, Chem. Rev. **116**, 8318 (2016).
[29] A. Drozdov, P. Kong, V. Minkov, S. Besedin, M. Kuzovnikov, S. Mozaffari, L. Balicas, F. Balakirev, D. Graf, V. Prakapenka *et al.*, Superconductivity at 250 K in lanthanum hydride under high pressures, Nature (London) **569**, 528 (2019).
[30] J. B. Goodenough, Theory of the role of covalence in the perovskite-type manganites [La, M(II)]MnO_3, Phys. Rev. **100**, 564 (1955).
[31] J. B. Goodenough, An interpretation of the magnetic properties of the perovskite-type mixed crystals $La_{1-x}Sr_xCoO_{3-\lambda}$, J. Phys. Chem. Solids **6**, 287 (1958).
[32] J. Kanamori, Superexchange interaction and symmetry properties of electron orbitals, J. Phys. Chem. Solids **10**, 87 (1959).
[33] V. M. Goldschmidt, Die gesetze der krystallochemie, Naturwissenschaften **14**, 477 (1926).
[34] Y. Goto, C. Tassel, Y. Noda, O. Hernandez, C. J. Pickard, M. A. Green, H. Sakaebe, N. Taguchi, Y. Uchimoto, Y. Kobayashi *et al.*, Pressure-stabilized cubic perovskite oxyhydride $BaScO_2H$, Inorg. Chem. **56**, 4840 (2017).
[35] See Supplemental Material at http://link.aps.org/supplemental/10.1103/PhysRevB.107.L140404 for details of the computational methods; discussions about competing phases for Na_2NiVH_6, determination of U values, and reliability of Curie temperature prediction; projected density of states (PDOS) for H in Na_2NiVH_6 and O in La_2NiMnO_6; phonon spectra of A_2NiVH_6 (A = Na, K, Rb, Cs) under 0 GPa and 10 GPa; equilibrated dynamical temperature plots versus time during *NVTab*

initio molecular dynamics simulations of Na_2NiVH_6 at 1200 K, 1400 K, and 1600 K; total and element resolved electronic band structures of A_2NiVH_6 at PBE_+U and HSE06 levels; density of states (DOS) and partial charge density at the conduction band minimum of Na_2NiVH_6 during *ab initio* molecular dynamics simulations after one electron inserted; the structures, energies, magnetic moments, DOSs, and averaged DOS of the nine Na_2NiVH_6 SQSs; Monte Carlo simulation input files for Na_2NiVH_6. This Supplemental Material includes Refs. [36–48].

[36] J. P. Perdew, K. Burke, and M. Ernzerhof, Generalized Gradient Approximation Made Simple, Phys. Rev. Lett. **77**, 3865 (1996).

[37] G. Kresse and J. Furthmüller, Efficient iterative schemes for *ab initio* total-energy calculations using a plane-wave basis set, Phys. Rev. B **54**, 11169 (1996).

[38] M. Zhu, Y. Lin, E. W. Lo, Q. Wang, Z. Zhao, and W. Xie, Electronic and magnetic properties of La_2NiMnO_6 and La_2CoMnO_6 with cationic ordering, Appl. Phys. Lett. **100**, 062406 (2012).

[39] Z. Fang, N. Nagaosa, and K. Terakura, Anisotropic optical conductivities due to spin and orbital ordering in $LaVO_3$ and YVO_3: First-principles studies, Phys. Rev. B **67**, 035101 (2003).

[40] P. E. Blöchl, Projector augmented-wave method, Phys. Rev. B **50**, 17953 (1994).

[41] J. Heyd, G. E. Scuseria, and M. Ernzerhof, Erratum: "Hybrid functionals based on a screened Coulomb potential" [J. Chem. Phys. **118**, 8207 (2003)], J. Chem. Phys. **124**, 219906 (2006).

[42] J. Heyd, G. E. Scuseria, and M. Ernzerhof, Hybrid functionals based on a screened Coulomb potential, J. Chem. Phys. **118**, 8207 (2003).

[43] A. Togo and I. Tanaka, First principles phonon calculations in materials science, Scr. Mater. **108**, 1 (2015).

[44] A. Van de Walle, P. Tiwary, M. De Jong, D. Olmsted, M. Asta, A. Dick, D. Shin, Y. Wang, L.-Q. Chen, and Z.-K. Liu, Efficient stochastic generation of special quasirandom structures, Calphad-Comput. Coupling Ph. Diagrams Thermochem. **42**, 13 (2013).

[45] P. S. Wang, W. Ren, L. Bellaiche, and H. J. Xiang, Predicting a Ferrimagnetic Phase of Zn_2FeOsO_6 with Strong Magnetoelectric Coupling, Phys. Rev. Lett. **114**, 147204 (2015).

[46] H. J. Xiang, S.-H. Wei, and M.-H. Whangbo, Origin of the Structural and Magnetic Anomalies of the Layered Compound $SrFeO_2$: A Density Functional Investigation, Phys. Rev. Lett. **100**, 167207 (2008).

[47] C. Huang, J. Feng, J. Zhou, H. Xiang, K. Deng, and E. Kan, Ultra-high-temperature ferromagnetism in intrinsic tetrahedral semiconductors, J. Am. Chem. Soc. **141**, 12413 (2019).

[48] C. Huang, J. Feng, F. Wu, D. Ahmed, B. Huang, H. Xiang, K. Deng, and E. Kan, Toward intrinsic room-temperature ferromagnetism in two-dimensional semiconductors, J. Am. Chem. Soc. **140**, 11519 (2018).

[49] Z. Deng, C.-J. Kang, M. Croft, W. Li, X. Shen, J. Zhao, R. Yu, C. Jin, G. Kotliar, S. Liu *et al.*, A pressure-induced inverse order-disorder transition in double perovskites, Angew. Chem. Int. Ed. **59**, 8240 (2020).

[50] H. L. Feng, Z. Deng, C. U. Segre, M. Croft, S. H. Lapidus, C. E. Frank, Y. Shi, C. Jin, D. Walker, and M. Greenblatt, High-pressure synthesis of double perovskite Ba_2NiIrO_6: In search of a ferromagnetic insulator, Inorg. Chem. **60**, 1241 (2020).

[51] A. Aimi, D. Mori, K.-i. Hiraki, T. Takahashi, Y. J. Shan, Y. Shirako, J. Zhou, and Y. Inaguma, High-pressure synthesis of A-site ordered double perovskite $CaMnTi_2O_6$ and ferroelectricity driven by coupling of A-site ordering and the second-order Jahn-Teller effect, Chem. Mater. **26**, 2601 (2014).

[52] H. Wu, W. Zhou, T. J. Udovic, J. J. Rush, and T. Yildirim, Crystal chemistry of perovskite-type hydride $NaMgH_3$: Implications for hydrogen storage, Chem. Mater. **20**, 2335 (2008).

[53] Y. Wang, J. Lv, L. Zhu, and Y. Ma, Crystal structure prediction via particle-swarm optimization, Phys. Rev. B **82**, 094116 (2010).

[54] Y. Wang, J. Lv, L. Zhu, and Y. Ma, CALYPSO: A method for crystal structure prediction, Comput. Phys. Commun. **183**, 2063 (2012).

[55] B. Gao, P. Gao, S. Lu, J. Lv, Y. Wang, and Y. Ma, Interface structure prediction via CALYPSO method, Sci. Bull. **64**, 301 (2019).

[56] T. Xie and J. C. Grossman, Crystal Graph Convolutional Neural Networks for an Accurate and Interpretable Prediction of Material Properties, Phys. Rev. Lett. **120**, 145301 (2018).

[57] G. Shirane, K. Suzuki, and A. Takeda, Phase transitions in solid solutions of $PbZrO_3$ and $PbTiO_3$(II) X-ray study, J. Phys. Soc. Jpn. **7**, 12 (1952).

[58] J. Lang, C. Li, X. Wang *et al.*, Improved photocatalytic performance under solar light irradiation by integrating wide-band-gap semiconductors, SnO_2, $SnTaO_3$ and $Sn_2Ta_2O_7$, Mater. Today: Proc. **3**, 424 (2016).

[59] H. Takatsu, O. Hernandez, W. Yoshimune, C. Prestipino, T. Yamamoto, C. Tassel, Y. Kobayashi, D. Batuk, Y. Shibata, A. M. Abakumov *et al.*, Cubic lead perovskite $PbMoO_3$ with anomalous metallic behavior, Phys. Rev. B **95**, 155105 (2017).

[60] F. Lou, X. Y. Li, J. Y. Ji, H. Y. Yu, J. S. Feng, X. G. Gong, and H. J. Xiang, PASP: Property analysis and simulation package for materials, J. Chem. Phys. **154**, 114103 (2021).

[61] M. Kitamura, I. Ohkubo, M. Matsunami, K. Horiba, H. Kumigashira, Y. Matsumoto, H. Koinuma, and M. Oshima, Electronic structure characterization of La_2NiMnO_6 epitaxial thin films using synchrotron-radiation photoelectron spectroscopy and optical spectroscopy, Appl. Phys. Lett. **94**, 262503 (2009).

[62] H. Wang, Q. Feng, X. Li, and J. Yang, High-throughput computational screening for bipolar magnetic semiconductors, Research (2022) 9857631.

[63] J. Li, X. Li, and J. Yang, A review of bipolar magnetic semiconductors from theoretical aspects, Fundam. Res. **2**, 511 (2022).

[64] H. Lv, X. Li, D. Wu, Y. Liu, X. Li, X. Wu, and J. Yang, Enhanced Curie temperature of two-dimensional Cr(II) aromatic heterocyclic metal-organic framework magnets via strengthened orbital hybridization, Nano Lett. **22**, 1573 (2022).

[65] X. Li, H. Lv, X. Liu, T. Jin, X. Wu, X. Li, and J. Yang, Two-dimensional bipolar magnetic semiconductors with high Curie-temperature and electrically controllable spin polarization realized in exfoliated $Cr(pyrazine)_2$ monolayers, Sci. China Chem. **64**, 2212 (2021).

[66] X. Li and J. Yang, First-principles design of spintronics materials, Natl. Sci. Rev. **3**, 365 (2016).

[67] X. Li and J. Yang, Bipolar magnetic materials for electrical manipulation of spin-polarization orientation, Phys. Chem. Chem. Phys. **15**, 15793 (2013).

[68] X. Li, X. Wu, Z. Li, J. Yang, and J. Hou, Bipolar magnetic semiconductors: A new class of spintronics materials, Nanoscale **4**, 5680 (2012).

[69] A. Zunger, S.-H. Wei, L. G. Ferreira, and J. E. Bernard, Special Quasirandom Structures, Phys. Rev. Lett. **65**, 353 (1990).

[70] K. Ueda, H. Tabata, and T. Kawai, Ferromagnetism in $LaFeO_3$-$LaCrO_3$ superlattices, Science **280**, 1064 (1998).

[71] J. E. Kleibeuker, E.-M. Choi, E. D. Jones, T.-M. Yu, B. Sala, B. A. MacLaren, D. Kepaptsoglou, D. Hernandez-Maldonado, Q. M. Ramasse, L. Jones *et al.*, Route to achieving perfect B-site ordering in double perovskite thin films, NPG Asia Mater. **9**, e406 (2017).

[72] D. Zhao, X. Wang, L. Chang, W. Pei, C. Wu, F. Wang, L. Zhang, J. Wang, and Q. Wang, Synthesis of super-fine $L1_0$-FePt nanoparticles with high ordering degree by two-step sintering under high magnetic field, J. Mater. Sci. Technol. **73**, 178 (2021).

[73] H. Wang, X. Ma, Y. He, S. Mitani, and M. Motokawa, Enhancement in ordering of FePt films by magnetic field annealing, Appl. Phys. Lett. **85**, 2304 (2004).

[74] J. Nag, D. Rani, J. Kangsabanik, D. Singh, R. Venkatesh, P. D. Babu, K. G. Suresh, and A. Alam, Bipolar magnetic semiconducting behavior in VNbRuAl, Phys. Rev. B **104**, 134406 (2021).